RAA 2016 Vol. **16** No. **1**, 13 (10pp) doi: 10.1088/1674–4527/16/1/013
http://www.raa-journal.org *http://iopscience.iop.org/raa*

***R**esearch in*
***A**stronomy and*
***A**strophysics*

The beaming effect and γ-ray emission for Fermi blazars

Yong-Yun Chen[1], Xiong Zhang †[1], Ding-Rong Xiong[2], Si-Ju Wang[3] and Xiao-Ling Yu[1]

[1] Department of Physics, Yunnan Normal University, Kunming 650500, China; *ynzx@yeah.net*
[2] Yunnan Observatories, Chinese Academy of Sciences, Kunming 650011, China
[3] Dongxing Middle School, Chuxiong 675000, China

Received 2015 May 1; accepted 2015 August 11

Abstract We study the γ-ray luminosity and beaming effect for Fermi blazars. Our results are as follows. (i) There are significant correlations between γ-ray luminosity and radio core luminosity, and between γ-ray luminosity and R_v, which suggests that the γ-ray emissions have a strong beaming effect. (ii) Using the $L_{\rm ext}/M_{\rm abs}$ as an indicator of environment effects, we find that there is no significant correlation between γ-ray luminosity and $L_{\rm ext}/M_{\rm abs}$ for all sources when we remove the effect of redshift. Flat spectrum radio quasars considered alone also do not show a significant correlation, but BL Lacertae objects (BL Lacs) still show a significant correlation when we remove the effect of redshift. These results suggest that the γ-ray emission may be affected by the environment on a kiloparsec scale for BL Lacs.

Key words: BL Lacerate objects: general — quasars: general — gamma-rays: galaxies — radio continuum: galaxies

1 INTRODUCTION

Blazars are an extreme subclass of active galactic nuclei (AGNs). According to observations, blazars show some extreme properties, namely, rapid variability, high optical polarization, high-energy γ-ray emission and superluminal motion (Angel & Stockman 1980; Wills et al. 1992; Stickel et al. 1993; Andruchow et al. 2005; Fan 2005; Gu et al. 2006).

Blazars are often divided into BL Lacertae objects (BL Lacs) and flat spectrum radio quasars (FSRQs) based on their emission line features. The FSRQs have strong emission lines, but BL Lacs have only very weak or non-existent emission lines. The classical divisions between FSRQs and BL Lacs are mainly based on the equivalent width (EW) of the emission lines. Those blazars with rest frame EW<5Å are classified as BL Lacs (e.g., Urry & Padovani 1995).

Many authors have found that there are many similar characteristics among FSRQs and BL Lacs, therefore most authors thought that they should be regarded as a single class which exhibits the behavior of blazars (Angel & Stockman 1980; Ghisellini et al. 2011; Giommi et al. 2012). However, some opponents argue that FSRQs and BL Lacs should not be treated as a single category due to the different emission lines that they emit. Ghisellini et al. (2009a) found that FSRQs and BL Lacs are well separated into two populations in the $\alpha_\gamma - L_\gamma$ plane, where α_γ and L_γ are the spectral index and γ-ray luminosity respectively. Ackermann et al. (2011) also confirmed this result.

Since the launch of the Fermi satellite, we have entered a new era of blazar research (Abdo et al. 2009, 2010). Up to now, the Large Area Telescope (LAT) has detected hundreds of blazars because it has higher sensitivity than EGRET in the 0.1–100 GeV energy range. However, questions about why some sources are γ-ray loud and others are gamma-ray quiet are still unclear. Doppler boosting is believed to be one of the important answers to these questions. Blazars detected by LAT are more likely to have larger Doppler factors (e.g., Lister et al. 2009; Savolainen et al. 2010). Linford et al. (2011) found that the difference between γ-ray loud and quiet FSRQs can be explained by Doppler boosting. The vast majority of LAT γ-ray sources are blazars, with strong, compact radio emission. These blazars show flat radio spectra and have compact cores with one-sided parsec-scale jets (Marscher 2006). Many authors suggest that the γ-ray emission originates from the jet and is also relativistically beamed, in the same manner as the radio emission (e.g., von Montigny et al. 1995; Mattox et al. 1993). The many correlations found between the γ-ray emissions detected by EGRET and the radio/mm-wave properties of blazars further support this scenario (Valtaoja & Terasranta 1995; Jorstad et al. 2001a,b; Lähteenmäki & Valtaoja 2003; Kellermann et al. 2004; Kovalev et al. 2005).

In this paper, we study the beaming effect and γ-ray emissions for Fermi blazars. The paper is structured as follows: we present the sample in Section 2; the results and discussion are described in Section 3; conclusions are drawn in Section 4.

2 DESCRIPTIONS OF THE SAMPLE AND DATA

A large number of blazars that have gamma-ray emission have been detected by Fermi LAT. The second LAT catalog (2LAC) contains 886 clean samples, comprising 395 BL Lacs, 310 FSRQs, 157 candidate blazars of unknown types, 8 misaligned AGNs, 4 narrow line Seyfert 1 galaxies, 10 AGNs of other types and 2 starburst galaxies (Ackermann et al. 2011). The most recent release is the third Fermi catalog of γ-ray sources, based on four years of data, consisting of 3033 sources (The Fermi-LAT Collaboration, 2015).

We tried to select a large number of blazars with reliable redshift, radio core and extended radio luminosity at 1.4 GHz. Firstly, we considered the following samples of blazars to get the radio core luminosity and extended luminosity at 1.4 GHz: Kharb et al. (2010), Antonucci & Ulvestad (1985), Cassaro et al. (1999), Murphy et al. (1993), Landt & Bignall (2008), Caccianiga & Marchã (2004), Giroletti et al. (2004). We also obtained the radio core luminosity at 1.4 GHz from NED for a few sources, which are not listed in the references in Table 1.

Secondly, we cross-correlated these samples with the Fermi LAT Third Source Catalog (3FGL), and we acquired the 3FGL spectral index and energy flux at 0.1–100 GeV from clean sources in 3FGL (Fermi-LAT Collaboration 2015)[1]. These clean sources are also included in the corresponding Second Catalog (2FGL).

Using these catalogs, we compiled 201 Fermi blazars. We used $L_v = 4\pi d_L^2 S_v$ to calculate the luminosity. The flux was k-corrected by $S_v = S_v^{\rm obs}(1+z)^{\alpha-1}$, where α is the spectral index, $\alpha^\gamma = \alpha^{\rm ph} - 1$, and $\alpha^{\rm ph}$ is the photon spectral index. The γ-ray luminosity can be calculated by the above equations.

The relevant data for Fermi blazars are listed in Table 1 with the following headings: column (1) the name of the sources in the catalog 3FGL; column (2) the classification of sources (BZB=BL Lac objects, BZQ=flat-spectrum radio quasars); column (3) redshift; column (4) apparent V-band magnitude obtained from the AGN catalog of Véron-Cetty & Véron (2006); column (5) the 3FGL photo-spectral index; column (6) the 3FGL gamma-ray energy flux in 0.1–100 GeV; column (7) the radio core flux at 1.4 GHz, whose unit is Jy; column (8) the extended radio flux at 1.4 GHz, whose unit is mJy; column (9) the references used for columns (7) and (8).

3 RESULTS AND DISCUSSION

3.1 The Distributions of Energy Spectral Index and γ-ray Luminosity

Figure 1 shows the energy spectral index as a function of redshift (left) and γ-ray luminosity as a function of redshift (right). We find that the energy spectral index does not have a significant dependence on redshift if blazar subclasses are considered separately. Ackermann et al. (2011) also found that no significant dependence of the photon index on redshift is observed if the subclasses of blazars are considered separately by using the blazars in 2LAC, as illustrated in figure 19 of Ackermann et al. (2011). Our result is contrary to the result of Ackermann et al. (2011). We find that there are significant correlations between spectral index and redshift for BL Lacs by using 3LAC (see Table 2). The γ-ray luminosity is plotted as a function of redshift in the right panel of Figure 1. A Malmquist bias is readily apparent in this figure as only high γ-ray luminosity sources (mostly FSRQs) are detected at large distances. Given their γ-ray luminosity distribution, most BL Lac objects could not be detected if they were located at redshifts greater than 1.

Figure 2 shows the γ-ray energy index versus γ-ray luminosity plane. From Figure 2, we can find that the spectral index vs γ-ray luminosity plane reveals a clear separation between FSRQs and BL Lacs. This correlation has been discussed in detail in the context of the "blazar divide" (Ghisellini et al. 2009a).

We find that most FSRQs have $L_\gamma > 10^{46}\ {\rm erg\ s^{-1}}$, but BL Lacs are below this value. Ghisellini et al. (2009a) suggested that it can be interpreted as a consequence of the changing accretion regime of the underlying accretion disk from radiatively efficient to inefficient, or, in other words, from a standard Shakura & Sunyaev (1973) disk to an advection dominated accretion flow (ADAF). We also find that most BL Lacs have a relatively flat α_γ ($\alpha_\gamma < 1.2$).

3.2 The γ-ray Luminosity vs Radio Core and Extended Luminosity

Figure 3 shows the γ-ray luminosity as a function of radio core luminosity (left) and γ-ray luminosity as a function of extended radio luminosity (right). We find a significant correlation between γ-ray luminosity and radio core luminosity for our sample (Table 2). Partial regression analysis also shows that the linear correlation between γ-ray luminosity and radio core luminosity is significant when the effects of redshift are removed ($r_{XY.Z}$=0.766, $P = 7.13 \times 10^{-33}$). This result suggests that γ-rays have a strong beaming effect.

Linford et al. (2011) found that γ-ray loud and γ-quiet objects are related to the core, and they suspected that the γ-ray radiation originates within the core (i.e., at the base of the jet). There is also a significant correlation between γ-ray luminosity and extended radio luminosity (Table 2). Partial regression analysis also shows that the linear correlation between γ-ray luminosity and extended radio luminosity is significantly correlated when the effects of redshift are removed ($r_{XY.Z} = 0.644$, $P = 7.31 \times 10^{-18}$). Fan et al. (2014) suggested that the γ-ray emissions are composed of two components: one is beamed, the other is unbeamed. The unbeamed part should be associated with the extended radio emissions. Recently, γ-ray emissions

[1] The 3FGL catalog is available at *http://fermi.gsfc.nasa.gov/ssc/data/access/lat/4yr_catalog*

Table 1 The Sample of Fermi Blazars

3FGL name	Class	Redshift	V	α_γ	$F_\gamma(\mathrm{erg\ s^{-1}\ cm^{-2}})$	$S_{\rm core}$	$S_{\rm ext}$	Ref
(1)	(2)	(3)	(4)	(5)	(6)	(7)	(8)	(9)
3FGL J0050.6–0929	BZB	0.2	17.44	2.0931	4.03071E-11	0.57	139.7	K10
3FGL J0108.7+0134	BZQ	2.099	18.39	2.260085	6.3754E-11	2.81	530.6	K10
3FGL J0112.1+2245	BZB	0.265	15.66	1.907256	7.77878E-11	0.36	3.9	K10
3FGL J0112.8+3207	BZQ	0.603	18.71	2.3626	3.87314E-11			
3FGL J0116.0–1134	BZQ	0.67	19	2.343904	1.51119E-11	0.65		
3FGL J0120.4–2700	BZB	0.559	16.21	1.914129	4.23886E-11		168	CB99
3FGL J0132.6–1655	BZQ	1.02	19.21	2.430135	2.61622E-11			
3FGL J0137.0+4752	BZQ	0.859	19.5	2.146481	5.10975E-11	1.88	8.7	K10
3FGL J0137.6–2430	BZQ	0.835	17.33	2.517637	1.53353E-11			
3FGL J0141.4–0929	BZB	0.733	17.5	2.122884	2.30759E-11		50	CB99
3FGL J0205.2–1700	BZQ	1.739	17.92	2.759468	1.82214E-11	0.61		
3FGL J0204.8+3212	BZQ	1.466	17.4	2.944624	1.05638E-11	0.65	11.7	K10
3FGL J0217.8+0143	BZQ	1.715	16.09	2.192922	4.61606E-11	0.45	71.1	K10
3FGL J0222.6+4301	BZB	0.444	15.2	1.879783	1.93512E-10	0.814	1052	A85
3FGL J0237.9+2848	BZQ	1.213	19.3	2.162098	1.11298E-10	2.33	99.9	K10
3FGL J0238.6+1636	BZB	0.94	15.5	2.057468	1.00162E-10	1.51	25.5	K10
3FGL J0252.8–2218	BZQ	1.419	20.41	2.152822	5.70612E-11			
3FGL J0259.5+0746	BZQ	0.893	17.51	2.212139	1.0597E-11	0.552	39	M93
3FGL J0315.5–1026	BZQ	1.565	19.71	2.410067	5.00533E-12			
3FGL J0339.5–0146	BZQ	0.852	18.41	2.252565	4.09816E-11	2.92	70.3	K10
3FGL J0340.5–2119	BZB	0.223	17.11	2.217488	7.18461E-12			
3FGL J0405.5–1307	BZQ	0.571	17.09	2.345819	6.40468E-12	4.33	9.1	K10
3FGL J0423.2–0119	BZQ	0.916	17	2.204462	5.95648E-11	2.91	70.2	K10
3FGL J0424.7+0035	BZB	0.31	16.98	2.197874	2.1339E-11	1.09	6.1	K10
3FGL J0428.6–3756	BZB	1.11	19	1.949819	1.83988E-10	0.68	86	CB99
3FGL J0442.6–0017	BZQ	0.844	17	2.495998	5.12195E-11	2.21		
3FGL J0449.0+1121	BZQ	1.375	19.81	2.233381	4.20064E-11	1.56	15.4	K10
3FGL J0449.4–4350	BZB	0.107	15.51	1.848965	1.2311E-10	0.0993	183.2	L08
3FGL J0453.2–2808	BZQ	2.559	18.51	2.630128	2.49535E-11			
3FGL J0501.2–0157	BZQ	2.286	18.06	2.413701	3.1127E-11	1.66	148.1	K10
3FGL J0505.3+0459	BZQ	0.954	18.71	2.463141	3.04786E-11	0.747		
3FGL J0530.8+1330	BZQ	2.06	20	2.245939	4.96196E-11	2.24	60.1	K10
3FGL J0532.7+0732	BZQ	1.254	19	2.203017	6.3002E-11	1.54	126.8	K10
3FGL J0538.8–4405	BZB	0.894	16.48	1.932384	3.08339E-10		220	CB99
3FGL J0608.0–0835	BZQ	0.872	17.6	2.372678	2.68982E-11	1.2	123.9	K10
3FGL J0611.1–6100	BZQ	1.773	20.71	2.704762	8.05141E-12			
3FGL J0630.9–2406	BZB	1.238	16	1.809364	4.28995E-11			
3FGL J0635.7–7517	BZQ	0.653	15.75	2.709976	2.04282E-11	0.21		
3FGL J0654.4+5042	BZQ	1.253	17.13	1.940565	1.58603E-11	0.31		
3FGL J0710.3+5908	BZB	0.125	15.71	1.661033	8.87552E-12	0.065	95	GM04
3FGL J0710.5+4732	BZB	1.292	14.51	2.647554	9.07156E-12	0.973	94	M93
3FGL J0721.9+7120	BZB	0.3	15.5	1.947768	2.12095E-10	0.69	376.4	K10
3FGL J0733.8+5021	BZQ	0.72	19.3	2.503782	6.41494E-12	0.69	82.5	K10
3FGL J0738.1+1741	BZB	0.424	16.22	2.006392	6.11881E-11	1.91	20.4	K10
3FGL J0739.4+0137	BZQ	0.189	16.47	2.245392	3.6569E-11	2.34	40.9	K10
3FGL J0749.0+4459	BZQ	0.192	16.31	2.371753	5.74985E-12	0.795	33.09	C04
3FGL J0750.6+1232	BZQ	0.889	18.7	2.411245	1.25277E-11	1.43	27	K10
3FGL J0757.0+0956	BZB	0.266	15	2.181859	2.11076E-11	2.07	6.7	K10
3FGL J0808.2–0751	BZQ	1.837	19.8	1.958395	8.5183E-11	1.58	59.8	K10
3FGL J0809.8+5218	BZB	0.138	15.21	1.876105	5.36237E-11	0.184	4.26	C04
3FGL J0811.3+0146	BZB	1.148	17.2	2.158473	2.77401E-11	0.46	18.2	K10
3FGL J0816.7+5739	BZB	0.054	17.41	2.112841	1.31154E-11	0.14	31.2	C04
3FGL J0826.0+0307	BZB	0.506	16.8	2.029678	5.84889E-12	1.32	4.1	K10
3FGL J0830.7+2408	BZQ	0.941	17.26	2.626917	1.89912E-11	0.76	62.7	K10
3FGL J0831.9+0430	BZB	0.174	16.4	2.096903	3.25377E-11	0.8	150.8	K10
3FGL J0834.1+4223	BZQ	0.249	17.81	2.439332	9.31559E-12	0.31		
3FGL J0841.4+7053	BZQ	2.172	17.3	2.616193	3.63477E-11	3.34	73.6	K10
3FGL J0839.5+0102	BZQ	1.123	19.31	2.237636	6.34951E-12	0.349		
3FGL J0849.3+0458	BZB	1.069	18.41	1.969532	5.94958E-12			
3FGL J0854.8+2006	BZB	0.306	15.43	2.122168	5.79991E-11	1.57	10.7	K10
3FGL J0903.1+4649	BZQ	1.465	18.66	2.614503	5.01679E-12	1.645	317	M93
3FGL J0909.1+0121	BZQ	1.025	17.31	2.457879	4.40967E-11	1	38	K10
3FGL J0909.8–0229	BZQ	0.957	18.81	2.101265	1.74076E-11			
3FGL J0915.8+2933	BZB	0.101	15.61	1.878973	2.34761E-11	0.222	111	A85
3FGL J0912.9–2104	BZB	0.198	15.81	1.94138	1.15942E-11			
3FGL J0916.3+3857	BZQ	1.267	19.61	2.356156	3.28224E-12	0.62		
3FGL J0920.9+4442	BZQ	2.19	18.16	2.13473	6.14445E-11	1.31		

Table 1 — *Continued.*

3FGL name	Class	Redshift	V	α_γ	$F_\gamma(\mathrm{erg\ s^{-1}\ cm^{-2}})$	$S_{\rm core}$	$S_{\rm ext}$	Ref
(1)	(2)	(3)	(4)	(5)	(6)	(7)	(8)	(9)
3FGL J0921.8+6215	BZQ	1.446	19.5	2.448463	1.58908E-11	1.11	6.4	K10
3FGL J0927.9–2037	BZQ	0.347	16.4	2.383753	7.41932E-12			
3FGL J0929.4+5013	BZB	0.37	16.91	2.164087	1.15974E-11	0.496	7.94	C04
3FGL J0945.9+5756	BZB	0.229	16.01	2.329607	7.22927E-12	0.069	9.01	C04
3FGL J0948.6+4041	BZQ	1.249	18.05	2.668701	5.58658E-12	1.23	95	K10
3FGL J0956.6+2515	BZQ	0.707	16.51	2.435683	1.21722E-11	0.483	19	M93
3FGL J0957.6+5523	BZQ	0.899	17.89	1.883193	9.58631E-11	2.568	381	M93
3FGL J0958.6+6534	BZB	0.368	16.81	2.38147	1.79248E-11	0.477	34	CB99
3FGL J1012.7+4229	BZB	0.364	17.21	1.663461	4.94324E-12	0.07	10	C04
3FGL J1015.0+4925	BZB	0.212	15.71	1.833418	8.86739E-11	0.39	12.31	C04
3FGL J1018.3+3542	BZQ	1.228	18.17	2.549106	4.29759E-12	0.9		
3FGL J1018.8+5913	BZB	2.025	17.21	2.090416	3.38454E-12	0.074	10.4	C04
3FGL J1031.2+5053	BZB	0.36	16.91	1.705211	1.13327E-11	0.038	1.25	C04
3FGL J1033.2+4116	BZQ	1.117	18.91	2.321686	1.56188E-11			
3FGL J1037.5+5711	BZB	0.83	17.31	1.720849	3.43411E-11	0.128	2.18	C04
3FGL J1053.7+4929	BZB	0.14	14.41	1.795846	7.04607E-12	0.052	16.6	C04
3FGL J1051.4+3941	BZB	0.498	19.41	1.664376	3.25784E-12			
3FGL J1058.5+0133	BZB	0.888	18.28	2.17084	6.53918E-11	2.7	230.8	K10
3FGL J1058.6+5627	BZB	0.144	14.61	1.94519	4.11866E-11	0.208	13.42	C04
3FGL J1104.4+3812	BZB	0.03	12.8	1.771642	3.82949E-10	0.52	181	A85
3FGL J1117.7–4632	BZQ	0.713	17.11	2.4303	8.24655E-12	0.27		
3FGL J1120.8+4212	BZB	0.124	17.51	1.616351	1.73008E-11	0.025	0.46	C04
3FGL J1127.0–1857	BZQ	1.05	18.65	2.116971	7.43853E-11	0.66	12.4	K10
3FGL J1129.9–1446	BZQ	1.184	16.9	2.786649	1.98472E-11	4.58	59.3	K10
3FGL J1136.6+6736	BZB	0.134	15.91	1.719091	7.88996E-12	0.04	10.7	C04
3FGL J1136.6+7009	BZB	0.046	11.61	1.823511	1.60471E-11	0.136	217.4	C04
3FGL J1143.0+6123	BZB	0.475	17.21	2.02133	9.51823E-12	0.066	3.52	C04
3FGL J1147.0–3811	BZB	1.048	16.2	2.253874	1.96677E-11		10	CB99
3FGL J1146.8+3958	BZQ	1.089	19.21	2.320755	4.11165E-11			
3FGL J1150.3+2417	BZB	0.2	16.81	2.212477	1.59886E-11	0.664	25	L08
3FGL J1151.4+5858	BZB	0.118	16.91	1.917273	9.18228E-12	0.137	55.2	C04
3FGL J1159.5+2914	BZQ	0.725	14.41	2.094657	8.3383E-11	1.55	196.1	K10
3FGL J1203.1+6029	BZB	0.066	12.41	2.208493	8.9288E-12	0.157	87.4	C04
3FGL J1204.3–0708	BZB	0.184	15.21	1.861201	1.23818E-11			
3FGL J1205.8–2636	BZQ	0.786	19.5	2.540616	1.17353E-11			
3FGL J1209.4+4119	BZB	0.377	17.61	1.944873	5.0527E-12	0.397	1.18	C04
3FGL J1217.8+3007	BZB	0.13	15.11	1.974478	6.80413E-11	0.355	189	A85
3FGL J1221.3+3010	BZB	0.182	16.31	1.660378	4.66783E-11	0.067	4.3	GM04
3FGL J1221.4+2814	BZB	0.102	14.91	2.102362	4.59189E-11	2.058	2.2	A85
3FGL J1222.4+0414	BZQ	0.966	17.98	2.508516	2.86599E-11	0.6	155.5	K10
3FGL J1224.9+2122	BZQ	0.432	17.5	2.185421	2.83853E-10	1.1	956.4	K10
3FGL J1224.6+4332	BZB	1.075	20.81	2.63592	6.86639E-12			
3FGL J1229.1+0202	BZQ	0.158	12.85	2.516284	1.80975E-10	34.89	17671	K10
3FGL J1231.7+2847	BZB	0.236	16.81	1.948491	3.09937E-11	0.06	26.3	
3FGL J1243.1+3627	BZB	1.065	17.01	1.768834	2.49859E-11	0.115	32.6	C04
3FGL J1246.7–2547	BZQ	0.633	17.31	2.139547	1.03318E-10			
3FGL J1248.2+5820	BZB	0.847	15.78	1.947429	4.50237E-11	0.18	4.2	C04
3FGL J1253.2+5300	BZB	0.445	17.51	1.897176	3.68671E-11	0.378	42.05	C04
3FGL J1256.1–0547	BZQ	0.536	17.75	2.232944	2.39182E-10	10.56	2095	K10
3FGL J1309.3+4304	BZB	0.69	17.11	1.935799	1.98727E-11	0.055	2.87	C04
3FGL J1310.6+3222	BZQ	0.998	15.24	2.152751	3.74705E-11	1.33	69.1	K10
3FGL J1317.8+3429	BZQ	1.056	18.21	2.583639	4.11444E-12	0.35		
3FGL J1326.8+2211	BZQ	1.4	18.9	2.333554	1.98206E-11	1.14	20.4	K10
3FGL J1337.6–1257	BZQ	0.539	19	2.366261	1.72496E-11	2.07	151	K10
3FGL J1351.1+0030	BZQ	2.084	21.81	2.312673	5.70342E-12			
3FGL J1355.0–1044	BZQ	0.332	18.4	2.386711	1.07919E-11			
3FGL J1417.8+2540	BZB	0.237	15.21	2.163691	3.9662E-12			
3FGL J1419.8+3819	BZQ	1.82	19.69	2.36463	7.65662E-12	0.52	2.5	K10
3FGL J1419.9+5425	BZB	0.153	15.65	2.307488	1.17707E-11	1.058	18	A85
3FGL J1427.0+2347	BZB	0.16	14.6	1.759839	1.48564E-10	0.25		
3FGL J1427.9–4206	BZQ	1.522	17.21	2.078681	1.79838E-10	1.37		
3FGL J1428.5+4240	BZB	0.129	15.01	1.574637	1.03283E-11	0.032	29.3	GM04
3FGL J1434.1+4203	BZQ	1.24	20.21	2.392054	4.77697E-12			
3FGL J1439.2+3931	BZB	0.344	17.1	1.770915	5.62814E-12	0.038		
3FGL J1442.8+1200	BZB	0.163	15.81	1.795514	6.93295E-12	0.06	8.5	GM04
3FGL J1454.5+5124	BZB	1.083	18.91	2.083831	2.68609E-11	0.08		
3FGL J1504.4+1029	BZQ	1.839	18.56	2.075091	2.43886E-10	1.82	38.3	K10
3FGL J1510.9–0542	BZQ	1.185	17.51	2.425565	2.69772E-11			

Table 1 — *Continued.*

3FGL name	Class	Redshift	V	α_γ	$F_\gamma(\mathrm{erg\ s^{-1}\ cm^{-2}})$	S_{core}	S_{ext}	Ref
(1)	(2)	(3)	(4)	(5)	(6)	(7)	(8)	(9)
3FGL J1512.8–0906	BZQ	0.36	16.54	2.304709	4.92754E-10	1.45	180.2	K10
3FGL J1516.9+1926	BZB	1.07	16.91	2.767541	6.01778E-12	0.255	1.7	A85
3FGL J1517.6–2422	BZB	0.049	13.21	2.112155	5.838E-11	2.562	32	A85
3FGL J1540.8+1449	BZB	0.605	17.3	2.344924	4.65077E-12	1.67	71.4	K10
3FGL J1542.9+6129	BZB	0.117	17.21	1.89592	4.48341E-11	0.126	3.7	C04
3FGL J1549.4+0237	BZQ	0.414	17.45	2.463335	2.48936E-11	1.15	18.8	K10
3FGL J1550.5+0526	BZQ	1.422	19.5	2.335909	1.57063E-11	2.21	42.9	K10
3FGL J1553.5+1256	BZQ	1.29	17.71	2.223356	2.99178E-11			
3FGL J1558.9+5625	BZB	0.3	17.81	2.209965	1.06152E-11	0.181	19.7	C04
3FGL J1607.0+1551	BZQ	0.497	18.11	2.284189	2.47804E-11			
3FGL J1608.6+1029	BZQ	1.226	18.7	2.619051	2.21968E-11	1.35	26.5	K10
3FGL J1613.8+3410	BZQ	1.399	18.11	2.351858	8.24224E-12	2.83	20.6	K10
3FGL J1635.2+3809	BZQ	1.813	18	2.414104	1.39949E-10	2.17	32	K10
3FGL J1637.7+4715	BZQ	0.74	17.91	2.367525	2.26393E-11			
3FGL J1640.6+3945	BZQ	1.66	19.37	2.28492	3.56168E-11	1.17	27.6	K10
3FGL J1653.9+3945	BZB	0.0337	13.78	1.716347	1.29752E-10	1.376	67	A85
3FGL J1700.1+6829	BZQ	0.301	19.01	2.398081	3.93633E-11	0.313		
3FGL J1719.2+1744	BZB	0.137	19.1	2.042681	1.75946E-11	0.661	11	A85
3FGL J1725.3+5853	BZB	0.297	17.1	2.178923	4.96372E-12	0.052	20.4	C04
3FGL J1728.5+0428	BZQ	0.296	18.31	2.594238	1.48769E-11	0.98		
3FGL J1727.1+4531	BZQ	0.717	18.1	2.346577	1.99875E-11	1	55.3	K10
3FGL J1728.3+5013	BZB	0.055	14.51	1.95986	1.22073E-11	0.175	50	A85
3FGL J1730.6+3711	BZB	0.204	17.1	2.08777	5.04089E-12	0.062	40.09	C04
3FGL J1733.0–1305	BZQ	0.902	19.5	2.244674	6.15628E-11	6.13	517.8	K10
3FGL J1740.3+5211	BZQ	1.375	18.7	2.452514	2.32386E-11	1.61	27.6	K10
3FGL J1743.9+1934	BZB	0.084	13.31	1.776926	7.95062E-12	0.157		
3FGL J1742.2+5947	BZB	0.4	17.31	2.301161	5.32817E-12	0.106	5	C04
3FGL J1749.1+4322	BZB	0.215	18.31	2.24691	1.3187E-11	0.235	19.5	C04
3FGL J1751.5+0939	BZB	0.322	16.78	2.118364	3.8702E-11	1.05	4.9	K10
3FGL J1748.6+7005	BZB	0.77	16.21	2.064401	4.59656E-11	0.61	12	CB99
3FGL J1801.5+4403	BZQ	0.663	17.9	2.695124	9.26074E-12	0.5	246.6	K10
3FGL J1800.5+7827	BZB	0.684	15.9	2.222699	5.86176E-11	1.98	20.8	K10
3FGL J1806.7+6949	BZB	0.051	14.22	2.234023	3.89695E-11	1.2	368.7	K10
3FGL J1813.6+3143	BZB	0.117	15.81	1.910873	1.12677E-11	0.074		
3FGL J1824.2+5649	BZB	0.664	19.3	2.459963	2.82805E-11	0.95	137.4	K10
3FGL J1829.4+5402	BZB	0.177	17.81	1.931645	7.22787E-12	0.018		
3FGL J1838.8+4802	BZB	0.3	16.81	1.806124	1.44346E-11	0.051	1.2	C04
3FGL J1849.2+6705	BZQ	0.657	16.9	2.142674	4.92003E-11	0.47	101	K10
3FGL J2001.0–1750	BZQ	0.65	18.6	2.309653	2.23784E-11	1.82	9.4	K10
3FGL J2000.0+6509	BZB	0.047	12.51	1.883226	6.81896E-11	0.2	60	GM04
3FGL J2005.2+7752	BZB	0.342	16.7	2.218685	2.06807E-11	0.823	28.9	M93
3FGL J2025.6–0736	BZQ	1.388	19.31	2.181554	7.29303E-11			
3FGL J2035.3+1055	BZQ	0.601	16.37	2.467874	2.50098E-11	0.781	40	A85
3FGL J2056.2–4714	BZQ	1.489	18.1	2.2647	7.73787E-11			
3FGL J2134.1–0152	BZB	1.285	19	2.207499	1.28413E-11	1.37	151.9	K10
3FGL J2143.5+1744	BZQ	0.211	15.73	2.403724	6.39508E-11	0.386		
3FGL J2147.2+0929	BZQ	1.113	18.54	2.377022	3.56426E-11	0.698	82	M93
3FGL J2158.0–1501	BZQ	0.672	18.3	2.26945	1.26202E-11	2.7	304.7	K10
3FGL J2158.8–3013	BZB	0.117	13.41	1.750328	2.30501E-10	0.252	132	A85
3FGL J2202.7+4217	BZB	0.069	14.72	2.161141	1.77287E-10	1.99	14.2	K10
3FGL J2203.4+1725	BZQ	1.075	19.5	2.152252	4.93254E-11	0.87	74.6	K10
3FGL J2212.0+2355	BZQ	1.125	20.66	2.212319	1.26704E-11	0.43	0.9	K10
3FGL J2217.0+2421	BZB	0.505	18.51	2.215108	1.09927E-11	0.42		
3FGL J2225.8–0454	BZQ	1.404	18.39	2.358605	2.47089E-11	7.13	91.6	K10
3FGL J2229.7–0833	BZQ	1.56	17.43	2.388687	5.40756E-11	0.93	8.4	K10
3FGL J2232.5+1143	BZQ	1.037	17.33	2.339162	7.26124E-11	6.99	148	K10
3FGL J2236.3+2829	BZQ	0.795	19.01	2.115377	4.35777E-11	1.118	3.4	M93
3FGL J2243.4–2541	BZB	0.774	17.81	2.274767	1.95586E-11			
3FGL J2254.0+1608	BZQ	0.859	16.1	1.634632	1.23418E-09	14.09	822	K10
3FGL J2258.0–2759	BZQ	0.927	16.77	2.173132	4.87036E-11	2.58		
3FGL J2258.3–5526	BZB	0.479	18.51	2.310879	3.16722E-12			
3FGL J2319.2–4207	BZB	0.054	14.81	2.095091	4.76094E-12	0.25	391.9	L08
3FGL J2334.1+0732	BZQ	0.401	16.04	2.504762	1.01509E-11	0.61	38.4	K10
3FGL J2338.1–0229	BZQ	1.072	19.01	2.495937	1.85497E-11			
3FGL J2348.0–1630	BZQ	0.576	18.41	2.202846	2.93969E-11	1.99	142.7	K10
3FGL J2359.3–3038	BZB	0.165	16.41	2.02159	6.61874E-12	0.039	27.2	GM04

Notes: The γ-ray fluxes and photon spectral indexes come from the 3FGL (Fermi-LAT Collaboration, 2015).

Table 2 Correlation Analysis

Param 1	Param 2	Class	Corr Coeff	Corr prob
(1)	(2)	(3)	(4)	(5)
L_γ	$L_{\rm core}$	All	0.921	1.84×10^{-68}
L_γ	$L_{\rm ext}$	All	0.855	7.65×10^{-42}
L_γ	$L_{\rm core}, z^*$	All	0.766	7.13×10^{-33}
L_γ	$L_{\rm ext}, z^*$	All	0.644	7.31×10^{-18}
L_γ	$R_{\rm c}$	All	0.176	0.041
L_γ	R_v	All	0.719	1.41×10^{-27}
L_γ	$[\log L_{\rm ext}]/M_{\rm abs}$	All	0.233	0.005
L_γ	$[\log L_{\rm ext}]/M_{\rm abs}, z^*$	All	0.078	0.356
		FSRQs	0.230	0.064
L_γ	$[\log L_{\rm ext}]/M_{\rm abs}, z^*$	FSRQs	-0.032	0.801
		BL Lacs	0.401	2.5×10^{-4}
L_γ	$[\log L_{\rm ext}]/M_{\rm abs}, z^*$	BL Lacs	0.24	0.034
L_γ	$M_{\rm abs}$	All	-0.715	9.55×10^{-33}
α_γ	z	FSRQs	0.016	0.869
		BL Lac	0.324	0.001

Notes: Columns (1) and (2) are parameters being examined for correlations. Results from a Pearson correlation analysis are cited in the main text. "$*$" is a Pearson partial correlation analysis excluding redshift. Significant correlation is identified when $P < 0.05$.

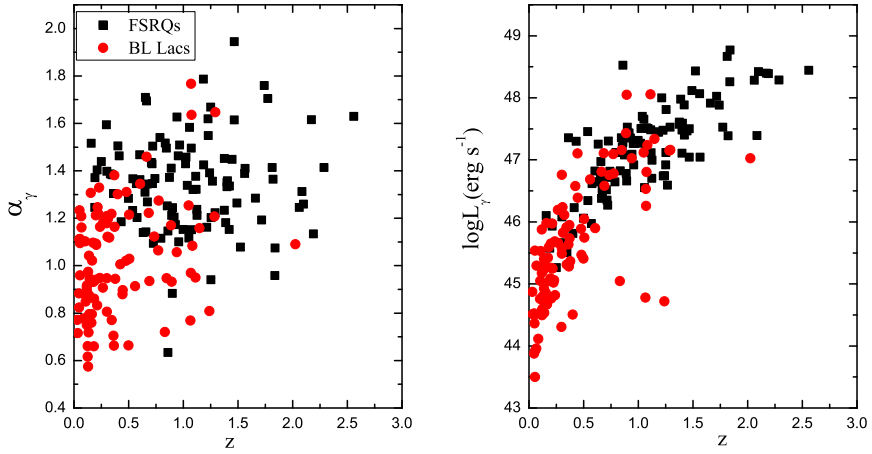

Fig. 1 The energy spectral index (*left*) and γ-ray luminosity (*right*) vs redshift for Fermi blazars. FSRQs: the black squares; BL Lacs: filled red circles (*color version is online*).

were detected from the lobe of Cen A (Massaro & Ajello 2011). Further investigation should be interesting.

3.3 The Beaming Effect

The ratio of the beamed radio core flux density ($S_{\rm core}$) to the unbeamed extended radio flux density ($S_{\rm ext}$), namely the radio core-dominance parameter ($R_{\rm c}$), has routinely been used as a statistical indicator of Doppler beaming and thereby orientation (Orr & Browne 1982; Kapahi & Saikia 1982; Kharb & Shastri 2004). The k-corrected $R_{\rm c}$ ($= \frac{S_{\rm core}}{S_{\rm ext}}(1+z)^{\alpha_{\rm core}-\alpha_{\rm ext}}$, with $\alpha_{\rm core} = 0$, $\alpha_{\rm ext} = 0.8$) is plotted against the γ-ray luminosity in Figure 4 (left). As expected, $R_{\rm c}$ is correlated with the γ-ray luminosity. However, we find that there is no significant correlation between $R_{\rm c}$ and γ-ray luminosity (Table 2). Fan et al. (2014) also found that there is no significant correlation between γ-ray luminosity and $R_{\rm c}$. But as we see below, the alternate orientation indicator, R_v, does show the expected behavior.

Wills & Brotherton (1995) defined R_v as the ratio of the radio core luminosity to the k-corrected absolute V-band magnitude ($M_{\rm abs}$): $\log R_v = \log \frac{L_{\rm core}}{L_{\rm opt}} = (\log L_{\rm core} + M_{\rm abs}/2.5) - 13.7$, where $M_{\rm abs} = M_V - k$ and the k-correction is k=$-2.5\log(1+z)^{1-\alpha_{\rm opt}}$ with the optical spectral index, $\alpha_{\rm opt} = 0.5$. Kharb et al. (2010) found that the ratio of the radio core luminosity to the k-corrected absolute V-band magnitude (R_v) is a better orientation indicator than $R_{\rm c}$ since optical luminosity is likely to be a better measure of intrinsic jet power than extended

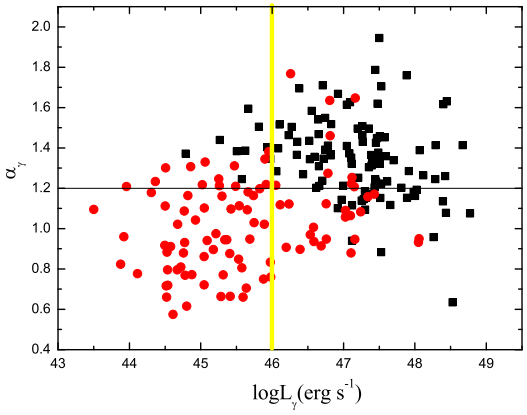

Fig. 2 Energy spectral index vs γ-ray luminosity for Fermi blazars. The black line is $\alpha_\gamma = 1.2$; the yellow line is $L_\gamma = 10^{46}$ erg s^{-1}. The meanings of different symbols are the same as in Fig. 1.

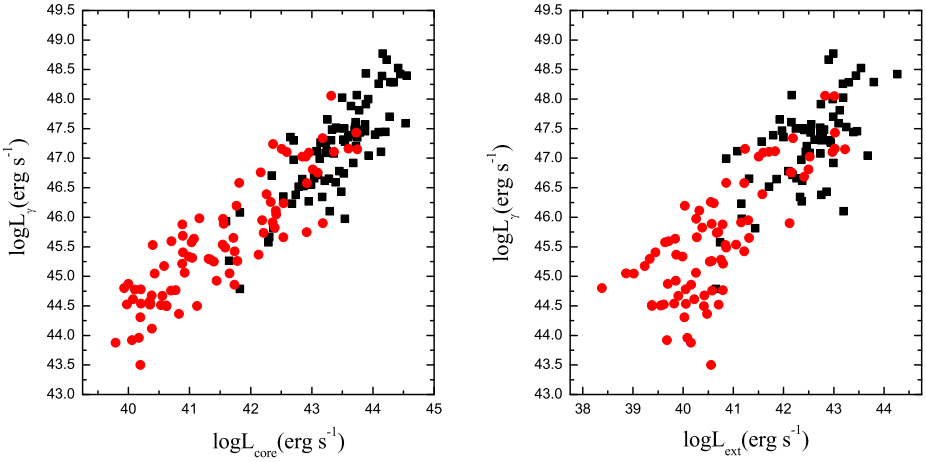

Fig. 3 The γ-ray luminosity vs core luminosity at 1.4 GHz (*left*) and extended luminosity at 1.4 GHz (*right*) for Fermi blazars. The meanings of different symbols are the same as in Fig. 1.

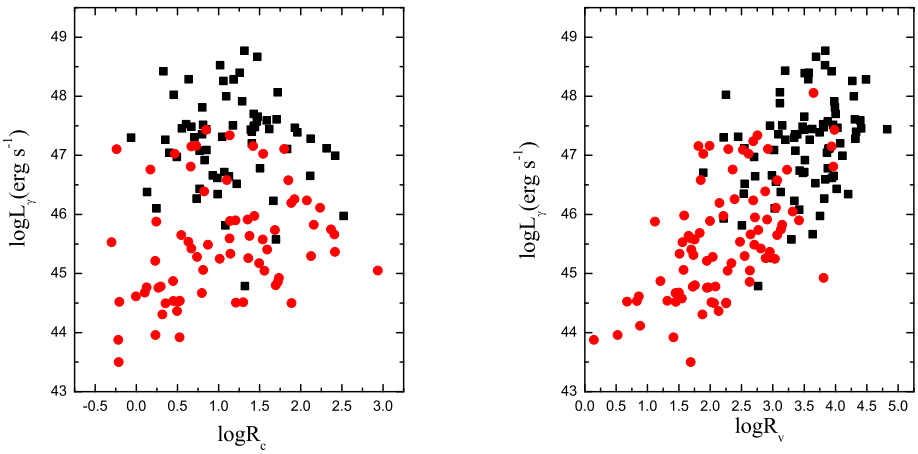

Fig. 4 The γ-ray luminosity vs orientation indicators, $R_{\rm c}$ (*left*) and R_v (*right*), for Fermi blazars. The meanings of different symbols are the same as in Fig. 1.

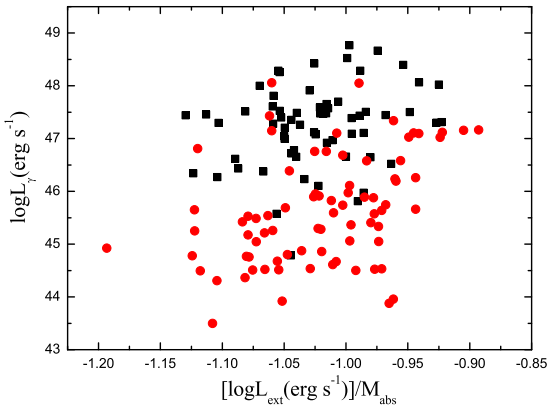

Fig. 5 The γ-ray luminosity vs the environment indicator for Fermi blazars. The meanings of different symbols are the same as in Fig. 1.

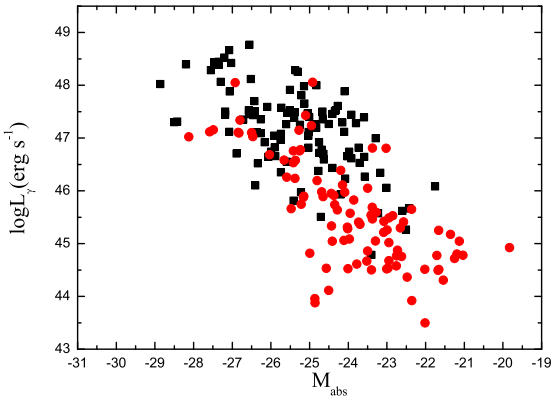

Fig. 6 The γ-ray luminosity vs absolute optical magnitude for Fermi blazars. The meanings of different symbols are the same as in Fig. 1.

radio luminosity (e.g., Maraschi et al. 2008; Ghisellini et al. 2009b). This is due to the fact that the optical continuum luminosity is correlated with the emission line luminosity over four orders of magnitude (Yee & Oke 1978), and the emission line luminosity is tightly correlated with the total kinetic power of the jet (Rawlings & Saunders 1991). The extended radio luminosity is suggested to be affected by interaction with the environment on kiloparsec scales. By making use of the above equations, we obtain R_v for our Fermi blazar sample. The γ-ray luminosity has a strong beaming effect.

Figure 4 suggests that R_v is indeed a better indicator of orientation as the correlation with γ-ray luminosity becomes stronger (see Table 2). Xiong et al. (2015) suggested that the Fermi and non-Fermi blazars have a significant difference in R_v. However, there is no significant difference in R_c for Fermi and non-Fermi blazars. These results indicate that R_v is a better orientation indicator than R_c.

3.4 The γ-ray Luminosity and Effect of the Environment

Kharb et al. (2010) proposed that if the extended radio luminosity is indeed affected by interaction with the kiloparsec scale environment and the optical luminosity is close to AGN power, the ratio $[\log L_{\rm ext}]/M_{\rm abs}$ can serve as a probe for environmental effects on kiloparsec scales (as suggested by Wills & Brotherton 1995). They used this ratio as the "environment indicator." According to the expression $[\log L_{\rm ext}]/M_{\rm abs}$, we obtain this "environment indicator."

Figure 5 shows the relation between γ-ray luminosity and $[\log L_{\rm ext}]/M_{\rm abs}$. We find that there is no significant correlation between them for all sources when the effect of redshift is removed (Table 2). The FSRQs considered alone also do not show a significant correlation, but the BL Lacs still show a significant correlation when the effect of redshift is removed (Table 2).

Ghisellini et al. (2011) suggested that the different properties between FSRQs and BL Lacs can be explained with the difference in jet power accompanied by a different environment, in turn caused by a different regime of accretion. FSRQs occur in the earlier phase. They have a powerful disk and jet, with high accretion. BL Lacs have a weak disk and weaker lines emitted closer to the black hole. Dense environments can decrease expansion losses in the source, but increase radiative losses, making the sources brighter at low radio frequencies (Barthel & Arnaud 1996). Because the environment around BL Lacs is not dense, it may lead to low accretion. The low accretion may cause low jet power. Ghisellini et al. (2011) also suggested that γ-ray luminosity is a good tracer for jet power in blazars. They pointed out that jets from BL Lac objects thus propagate in a medium starved of external radiation (weak disk and weak lines), and this makes the emitting electrons accelerate in the jet cool less and reach very high energies. Their emitted high energy spectrum, produced mainly by the synchrotron self-Compton mechanism, is less luminous and harder than in FSRQs. The latter sources in fact have a radiatively efficient accretion disk and a corresponding standard broad line region. If the jet dissipates most of its power within the broad line region, then the emitting electrons will efficiently cool (mostly by external Compton), reach only moderate energies, and produce a high energy peak below 100 MeV. Generally, BL Lacs have lower γ-ray luminosity than FSRQs. Zhang et al. (2014) have suggested that the dominant formation mechanism of FSRQ jets may be the Blandford-Znajek (BZ) process, but BL Lac object jets may be produced via the Blandford-Payne (BP) and/or BZ processes, depending on the structures and accretion rates of accretion disks. The BP mechanism may power a jet by releasing the gravitational energy of accreting matter that moves toward the black hole (BH). The rotational energy of a rapidly rotating BH is essential for the BZ process. Ineson et al. (2015) have suggested that jet and environment have strong correlations for low accretion radio loud AGNs but not for high

accretion radio loud AGNs. We know that the FSRQs are high accretion radio loud AGNs, and the BL Lacs are low accretion radio loud AGNs. Moreover, we find that there is a significant correlation between γ-ray luminosity and the environment indicator for BL Lacs, but not for FSRQs. These results therefore may suggest that the γ-ray emissions are affected by the environment on kiloparsec scales for BL Lacs.

Figure 6 shows the relation between γ-ray luminosity and absolute magnitude. We find a significant anti-correlation between them (Table 2). This figure shows a similar "blazar sequence." Fossati et al. (1998) and Ghisellini et al. (1998) have proposed the so-called "blazar sequence" with plots of various powers vs the synchrotron peak frequency for a sample of blazars containing FSRQs and BL Lacs. This sample showed an anti-correlation with the most powerful sources having relatively small synchrotron peak frequencies and the least powerful ones having the highest $\nu_{\rm peak}$ (Wu et al. 2009).

4 CONCLUSIONS

From our results and discussions mentioned above, we can conclude that: (i) There are significant correlations between γ-ray luminosity and both radio core luminosity and R_v, which suggests that the γ-ray luminosity has a strong beaming effect. (ii) Using the $L_{\rm ext}/M_{\rm abs}$ as an indicator of environment effects, FSRQs considered alone do not show a significant correlation, but BL Lacs still show a significant correlation when we remove the effect of redshift. These results suggest that the γ-ray emission may be affected by the environment on a kiloparsec scale for BL Lacs.

Acknowledgements We thank the anonymous referee for valuable comments and suggestions. We are very grateful to the Science Foundation of Yunnan Province of China (Grant Nos. 2012F13140 and 2010CD046). This work is supported by the National Natural Science Foundation of China (Grant Nos. 11063004, 11163007 and U1231203), and the High-Energy Astrophysics Science and Technology Innovation Team of Yunnan Higher School and Yunnan Gravitation Theory Innovation Team (2011c1). This work is supported by the research innovation fund for graduate students, Yunnan Normal University (yjs201566). This research has made use of the NASA/IPAC Extragalactic Database (NED), that is operated by Jet Propulsion Laboratory, California Institute of Technology, under contract with the National Aeronautics and Space Administration.

References

Abdo, A. A., Ackermann, M., Ajello, M., et al. 2009, ApJ, 700, 597
Abdo, A. A., Ackermann, M., Ajello, M., et al. 2010, ApJ, 715, 429
Ackermann, M., Ajello, M., Allafort, A., et al. 2011, ApJ, 743, 171
Andruchow, I., Romero, G. E., & Cellone, S. A. 2005, A&A, 442, 97
Angel, J. R. P., & Stockman, H. S. 1980, ARA&A, 18, 321
Antonucci, R. R. J., & Ulvestad, J. S. 1985, ApJ, 294, 158
Barthel, P. D., & Arnaud, K. A. 1996, MNRAS, 283, L45
Caccianiga, A., & Marchã, M. J. M. 2004, MNRAS, 348, 937 (C04)
Cassaro, P., Stanghellini, C., Bondi, M., et al. 1999, A&AS, 139, 601 (CB99)
Fan, J.-H. 2005, Chinese Journal of Astronomy and Astrophysics Supplement, 5, 213
Fan, J. H., Yang, J. H., Wu, D. X., et al. 2014, in IAU Symposium, 304, eds. A. M. Mickaelian, & D. B. Sanders, 157
Fossati, G., Maraschi, L., Celotti, A., Comastri, A., & Ghisellini, G. 1998, MNRAS, 299, 433
Ghisellini, G., Celotti, A., Fossati, G., Maraschi, L., & Comastri, A. 1998, MNRAS, 301, 451
Ghisellini, G., Maraschi, L., & Tavecchio, F. 2009a, MNRAS, 396, L105
Ghisellini, G., Tavecchio, F., & Ghirlanda, G. 2009b, MNRAS, 399, 2041
Ghisellini, G., Tavecchio, F., Foschini, L., & Ghirlanda, G. 2011, MNRAS, 414, 2674
Giommi, P., Padovani, P., Polenta, G., et al. 2012, MNRAS, 420, 2899
Giroletti, M., Giovannini, G., Taylor, G. B., & Falomo, R. 2004, ApJ, 613, 752 (GM04)
Gu, M. F., Lee, C.-U., Pak, S., Yim, H. S., & Fletcher, A. B. 2006, A&A, 450, 39
Ineson, J., Croston, J. H., Hardcastle, M. J., et al. 2015, arXiv:1508.01033
Jorstad, S. G., Marscher, A. P., Mattox, J. R., et al. 2001a, ApJ, 556, 738
Jorstad, S. G., Marscher, A. P., Mattox, J. R., et al. 2001b, ApJS, 134, 181
Kapahi, V. K., & Saikia, D. J. 1982, Journal of Astrophysics and Astronomy, 3, 465
Kellermann, K. I., Lister, M. L., Homan, D. C., et al. 2004, ApJ, 609, 539
Kharb, P., Lister, M. L., & Cooper, N. J. 2010, ApJ, 710, 764 (K10)
Kharb, P., & Shastri, P. 2004, A&A, 425, 825
Kovalev, Y. Y., Kellermann, K. I., Lister, M. L., et al. 2005, AJ, 130, 2473
Lähteenmäki, A., & Valtaoja, E. 2003, ApJ, 590, 95
Landt, H., & Bignall, H. E. 2008, MNRAS, 391, 967 (L08)
Linford, J. D., Taylor, G. B., Romani, R. W., et al. 2011, ApJ, 726, 16
Lister, M. L., Homan, D. C., Kadler, M., et al. 2009, ApJ, 696, L22
Maraschi, L., Foschini, L., Ghisellini, G., Tavecchio, F., & Sambruna, R. M. 2008, MNRAS, 391, 1981

Marscher, A. P. 2006, in American Institute of Physics Conference Series, 856, Relativistic Jets: The Common Physics of AGN, Microquasars, and Gamma-Ray Bursts, eds. P. A. Hughes, & J. N. Bregman, 1
Massaro, F., & Ajello, M. 2011, ApJ, 729, L12
Mattox, J. R., Bertsch, D. L., Chiang, J., et al. 1993, ApJ, 410, 609
Murphy, D. W., Browne, I. W. A., & Perley, R. A. 1993, MNRAS, 264, 298 (M93)
Orr, M. J. L., & Browne, I. W. A. 1982, MNRAS, 200, 1067
Rawlings, S., & Saunders, R. 1991, Nature, 349, 138
Savolainen, T., Homan, D. C., Hovatta, T., et al. 2010, A&A, 512, A24
Shakura, N. I., & Sunyaev, R. A. 1973, A&A, 24, 337
Stickel, M., Fried, J. W., & Kuehr, H. 1993, A&AS, 98, 393
Urry, C. M., & Padovani, P. 1995, PASP, 107, 803
Valtaoja, E., & Terasranta, H. 1995, A&A, 297, L13
Véron-Cetty, M.-P., & Véron, P. 2006, A&A, 455, 773
von Montigny, C., Bertsch, D. L., Chiang, J., et al. 1995, ApJ, 440, 525
Wills, B. J., & Brotherton, M. S. 1995, ApJ, 448, L81
Wills, B. J., Wills, D., Breger, M., Antonucci, R. R. J., & Barvainis, R. 1992, ApJ, 398, 454
Wu, Z.-Z., Gu, M.-F., & Jiang, D.-R. 2009, RAA (Research in Astronomy and Astrophysics), 9, 168
Xiong, D., Zhang, X., Bai, J., & Zhang, H. 2015, MNRAS, 451, 2750
Yee, H. K. C., & Oke, J. B. 1978, ApJ, 226, 753
Zhang, J., Sun, X. N., Liang, E. W., et al. 2014, ApJ, 788, 104